RSC Advances

PAPER

View Article Online
View Journal | View Issue

Cite this: *RSC Adv.*, 2017, **7**, 49353

Growth, characterization, and thin film transistor application of $CH_3NH_3PbI_3$ perovskite on polymeric gate dielectric layers†

Jenner H. L. Ngai,‡[ab] Johnny K. W. Ho,‡[a] Rocky K. H. Chan,[a] S. H. Cheung,[a] Louis M. Leung[b] and S. K. So*[a]

Methylammonium-based perovskite compounds are generally grown on conducting or semiconducting substrates for high performance solar cell applications. In this study, we explore the growth of these compounds on insulators and test for their field-effect transistor performance. The key challenge is to find a surface that favors the crystal growth of perovskites without compromising the adhesion of the crystals. A family of methacrylate-based polymers has been identified as the insulators. Onto these insulators, methylammonium lead iodide polycrystalline thin films were grown. Generally, we found that the crystal size in the perovskite layers is well-correlated with the surface hydrophobicity. More hydrophobic polymer layers favor the growth of larger crystals, but result in less favorable adhesion of the perovskite. Methacrylate polymers with a phenyl substituent can give better adhesion and crystal sizes despite their hydrophobic properties. Among the different insulating polymer layers, we found that poly(phenyl methacrylate) (PPhMA), a derivative of the common commercial plastic poly(methyl methacrylate) (PMMA), produces the best perovskite films. The molecular origin of these properties is discussed. To test the electronic properties of these films, we employed them for thin-film transistor applications. Under optimal conditions, the thin-film transistors fabricated on PPhMA produce the best device with an electron mobility of 0.4 $cm^2\ V^{-1}\ s^{-1}$. Our results are also supported by photothermal deflection spectroscopy investigations of the subgap optical absorptions of these films.

Received 6th August 2017
Accepted 9th October 2017

DOI: 10.1039/c7ra08699g

rsc.li/rsc-advances

1 Introduction

Solution processable organic–inorganic hybrid perovskite films have become probably the most hotly contended material in photovoltaics (PV) within a short span of a few years.[1–3] Power conversion efficiencies (PCEs) of perovskite-based solar cells have surged from 3.8 to 22.1% and more.[4] As high quality polycrystalline thin films of perovskites are essential for PV devices with stable and high PCEs,[5] numerous studies have already been devoted to the study of the growth of perovskite films on conducting or semiconducting surfaces.[6]

Besides PV applications, perovskites should be identified as a multi-functional electronic material.[7–10] Several properties make the multi-functionality appealing. These include sharp optical bandedge,[7] small exciton binding energy,[8] long carrier lifetime,[9] and high charge carrier mobility[10] to name a few. These outstanding optoelectronic properties should position perovskite compounds for use in a wide range of devices beyond solar cells. Conceivable examples are photodetectors, lasers, light-emitting diodes, and thin-film transistors (TFTs). The key advantages of perovskite TFTs are their potential to achieve high mobility and processability. Most high performance OTFT materials have semi-crystalline structures or favorable intermolecular packing which enables effective charge hopping,[11] and these require carefully designed molecular structures and specific processing conditions.[12,13] Compared to pure OTFTs, it is relatively easier to obtain high crystallinity perovskite-based transistor materials. A hole mobility of >100 $cm^2\ V^{-1}\ s^{-1}$ and electron mobility of >20 $cm^2\ V^{-1}\ s^{-1}$ have been revealed in methylammonium lead iodide perovskite single crystals,[9] and the intrinsic mobility limited by the acoustic phonon scattering can go up to a few thousand $cm^2\ V^{-1}\ s^{-1}$.[14] Perovskite materials can also be solution processed, which is particularly suitable for printed electronics.[15]

Despite the appealing potential breakthrough offered by perovskite materials, the applications in TFT are still quite limited.[16–20] One of the key hurdles for the fabrication of TFTs is the identification of a suitable dielectric layer for the growth of

[a]*Department of Physics and Institute for Advanced Materials, Hong Kong Baptist University, Kowloon Tong, Hong Kong, China. E-mail: skso@hkbu.edu.hk*

[b]*Department of Chemistry, Hong Kong Baptist University, Kowloon Tong, Hong Kong, China*

† Electronic supplementary information (ESI) available. See DOI: 10.1039/c7ra08699g

‡ These authors contributed equally to this work.

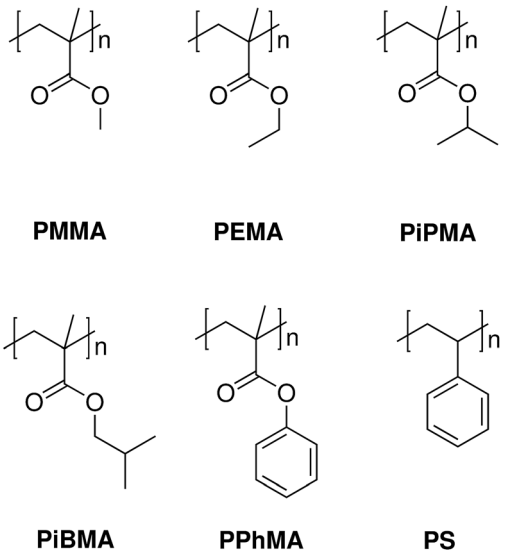

Fig. 1 The polymers used to study the growth of the perovskite on different hydrophobic surfaces.

perovskite crystals.[21,22] This hurdle is especially challenging for solution processable perovskite films for TFTs. Broadly speaking, gate dielectric layers can either be hydrophilic or hydrophobic. For a hydrophilic gate dielectric layer, perovskites are known to adhere favorably.[23] However, the strong interactions between the gate layer and perovskite prevent the growth of large crystals at the interface. The presence of small crystallite hinders charge carrier transport along the conducting channel, and results in poor TFT performance. For a hydrophobic dielectric, the wetting of the perovskite from a solution precursor is poor, and thus forbids the growth of any continuous films, which is essential for TFTs. Thus, a compromise must be made in terms of the hydrophobicity of the underlying gate dielectric layer.

In this contribution, we identified several polymeric methacrylate (MA)-based polymers, and characterized their thin film hydrophobicities. We then grew methylammonium lead iodide ($CH_3NH_3PbI_3$) perovskite films on these polymers using solution processing techniques. The methacrylate polymers chosen were poly(methyl methacrylate) (PMMA), poly(ethyl methacrylate) (PEMA), poly(isopropyl methacrylate) (PiPMA), poly(isobutyl methacrylate) (PiBMA) and poly(phenyl methacrylate) (PPhMA). They possess sound thermal and chemical stability, and are available commercially. The series of methacrylate polymers also provides a systematic way to study how surface hydrophobicity affects the growth of perovskites. Besides these five polymers, polystyrene (PS) was also examined as a control in order to demonstrate the role of the methacrylate functional group in the growth of the perovskite films. The chemical structures of all these polymers are shown in Fig. 1. We found a clear correlation between the hydrophobicity and the size and qualities of the perovskite crystals. Furthermore, we demonstrate how to use these perovskite films to fabricate bottom-gate top-contact TFTs having a highest mobility of about 0.40 $cm^2 V^{-1} s^{-1}$.

2 Experimental

Lead(II) iodide 99% (PbI_2), poly(methyl methacrylate) (PMMA), poly(ethyl methacrylate) (PEMA), poly(isobutyl methacrylate) (PiBMA), poly(phenyl methacrylate) (PPhMA), and polystyrene (PS) were purchased from Sigma Aldrich. Poly(isopropyl methacrylate) (PiPMA) was purchased from Polysciences, Inc. Methylammonium iodide (MAI) was purchased from Tokyo Chemical Industry Co., Ltd (TCI). PbI_2 was dissolved in dimethylformamide (DMF) in a concentration of 450 mg mL^{-1} and stirred at 70 °C overnight. MAI was dissolved in isopropanol at a concentration of 45 mg mL^{-1} and stirred at 70 °C overnight. All perovskite films were grown on heavily p-doped silicon substrates which were thermally grown with 300 nm of SiO_2. The substrates were washed by sonication in deionized water, acetone, methanol and isopropanol followed by ultraviolet-ozone treatment. Afterwards, polymer solutions in chlorobenzene were spin-coated onto the substrates and dried at 100 °C for 1 hour in a nitrogen-filled glovebox. The dried polymer films served as the substrate layer for the growth of the perovskite films. We employed a 2-step approach to grow the perovskite films. Firstly, PbI_2 dissolved in DMF was spin-coated on top of the polymer layer at 1200 rpm for 60 s and was subsequently annealed at 70 °C for 1 hour. Solvent annealing was carried out using the same conditions with 10 μL of DMF droplets next to the samples, and covered with a glass Petri dish during the solvent annealing. Secondly, the MAI solution in isopropanol was then deposited onto the PbI_2 layer at 1200 rpm for 60 s. Finally, thermal and solvent annealing were performed on the samples using a similar procedure described above except the temperature for annealing was 100 °C.

The hydrophobicity of the polymer films was investigated by contact angle measurements. The measurements were carried out using a digital camera to capture an image of a 5.0 μL water droplet on the thin-film polymer. The contact angle is the angle between the tangent of the water droplet and the wafer surface. The morphologies of the perovskite films were investigated using scanning electron microscopy (SEM) (LEO Gemini 1530). The average crystal size of the perovskite crystals on different polymers was calculated automatically by the software ImageJ using the SEM images of the perovskite crystal grains captured at 10000× magnification. The crystallinity of the films was evaluated using grazing incidence X-ray diffraction (GIXRD) with a Bruker AXS D8 Advance X-ray Diffractometer. The perovskite films with satisfactory crystal qualities were further used for thin-film transistor (TFT) fabrication. A bottom-gate top-contact architecture was employed for the TFTs. Gold (100 nm) source (S) and drain (D) electrodes were deposited *via* thermal evaporation through a shadow mask, defining a channel length (L) of 50 μm and a channel width (W) of 6 mm. The electrical performance measurements of the TFT devices were carried out in a cryostat (Oxford Instruments, Optistat DN-V) under high vacuum (10^{-5} Torr) and dark conditions at various temperatures and measured by a Keithley 236 source measurement unit together with a Xantrex XT 120-0.5 as the DC gate voltage supply.

3 Results and discussion

3.1 Perovskite film growth on the polymeric insulators

Contact angle analysis of the polymeric insulators. The surface hydrophobicity of the polymers was assessed by contact angle measurements. The contact angle and thus the hydrophobicity of the polymers increases in the following order: PMMA < PEMA < PiPMA ≈ PPhMA < PiBMA < PS (Fig. 2). Among the MA series of polymers, PMMA is the least hydrophobic while PiBMA is the most hydrophobic. Replacing the methyl group in PMMA with bulkier alkyl or aromatic groups enhances the hydrophobicity. Thus exposure of the O atoms in the MA groups affects the hydrophobicity of the polymer films. Shielding these O atoms with hydrophobic alkyl or phenyl groups (as in PEMA, PiPMA, PiBMA, and PPhMA) would suppress the hydrophilicity (and enhance the hydrophobicity). Thus, those polymers clearly offer a means to evaluate the relationship between substrate hydrophobicity and perovskite crystal growth using solution processing.

Morphologies of the perovskite films. Methylammonium lead iodide ($CH_3NH_3PbI_3$) was deposited on the different polymers *via* the 2-step perovskite solution process outlined in Part 2. Fig. 3 shows the scanning electron microscopy (SEM) images of these perovskite films. In the MA polymer series [Fig. 3(a)–(e)], compact polycrystalline films can be clearly observed on all the MA polymer layers, with the exceptions of the PiPMA and PiBMA surfaces [Fig. 3(c) and (d)]. Close-up SEM images in the insets of Fig. 3 further reveal the shapes and contacts between the crystals. For the polymer surfaces with larger crystals, the grains develop straight edges [*e.g.* Fig. 3(e)]. Furthermore, the grain boundaries in between crystallites appear to be tighter. Fig. 4(a) presents a summary of the average crystal sizes (area) on different polymers. Of all the polymer layers, the perovskite crystals grown on the least hydrophobic PMMA have the smallest crystallites, with an average dimension of about 0.15 μm^2, and an island geometry [Fig. 3(a)]. In contrast, the more hydrophobic PEMA and PPhMA surfaces support larger crystal growth [Fig. 3(b) and (e)]. For PPhMA, the average crystal dimension is about 1.15 μm^2, which is about 8 times larger than the crystals on PMMA. Fig. 4(b)–(d) compare the detailed size distribution of the crystals on the MA polymers, with the characteristic GIXRD patterns of the films in the ESI confirming the perovskite crystals. It can be seen that there is a correlation between the hydrophobicity and the size of the perovskite crystals. More hydrophobic MA polymers favor the growth of larger crystals, but for the hydrophobic PiPMA and PiBMA surfaces, the adhesions are poor [Fig. 3(c) and (d)]. In addition, despite the similar hydrophobicity of PiPMA and PPhMA, PPhMA gives a well-wetted perovskite film but PiPMA gives a poorly-wetting surface. These essentially promote a motivation of understanding of crystal growth beyond surface hydrophobicity.

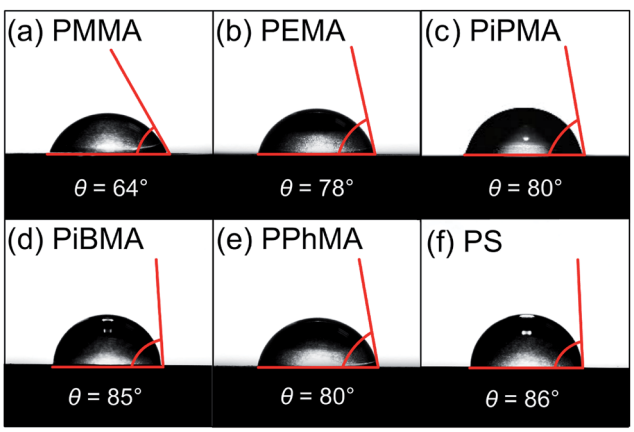

Fig. 2 Contact angles of a water droplet on the polymer substrates: (a) PMMA; (b) PEMA; (c) PiPMA; (d) PiBMA; (e) PPhMA and (f) PS.

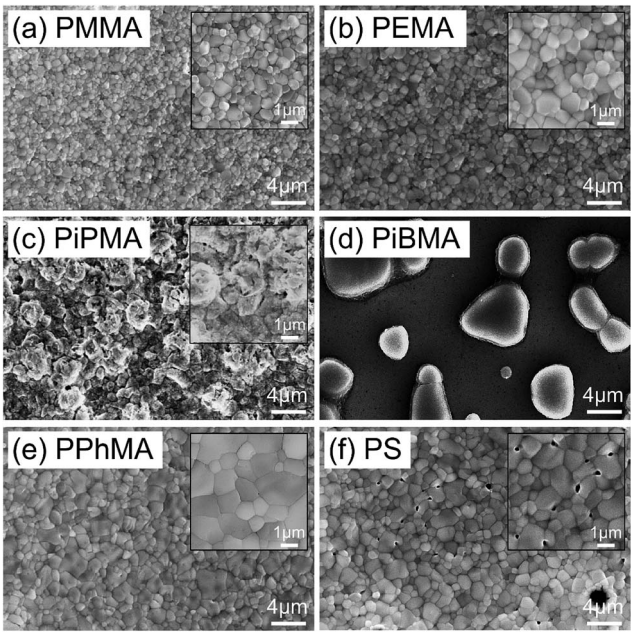

Fig. 3 SEM images of the perovskite crystals on the polymer substrates: (a) PMMA; (b) PEMA; (c) PiPMA (poor wetting, non-uniform film); (d) PiBMA (non-wetting); (e) PPhMA and (f) PS (poor adhesion with physical pinholes).

Below, we briefly discuss the molecular origin of crystal growth on the MA polymers based on the criterion of adhesion in relation to hydrophobicity and how it influences perovskite crystal growth. In the MA polymers, electronegative oxygen atoms and some side groups as substituents attached to the oxygen atoms can be found. An adhesion contribution by the hydrophilic O atoms can be revealed from a control experiment of the growth of perovskite crystals on PS in which O atoms are missing. Surprisingly, comparing PPhMA and PS, perovskite crystals with an average size of 0.57 μm^2 can be observed on the PS surface with numerous pinholes, as revealed by the SEM image [Fig. 3(f)], indicating that the crystals might not adhere well on the hydrophobic PS surface. From this, we postulate that the O atoms in the MA group provide initial nucleation sites to the polymer and give better adhesion. A similar observation was reported recently by Grätzel *et al.* who suggested that the methacrylate moiety can act as a support and scaffold to induce nucleation of the perovskite crystal growth.[1]

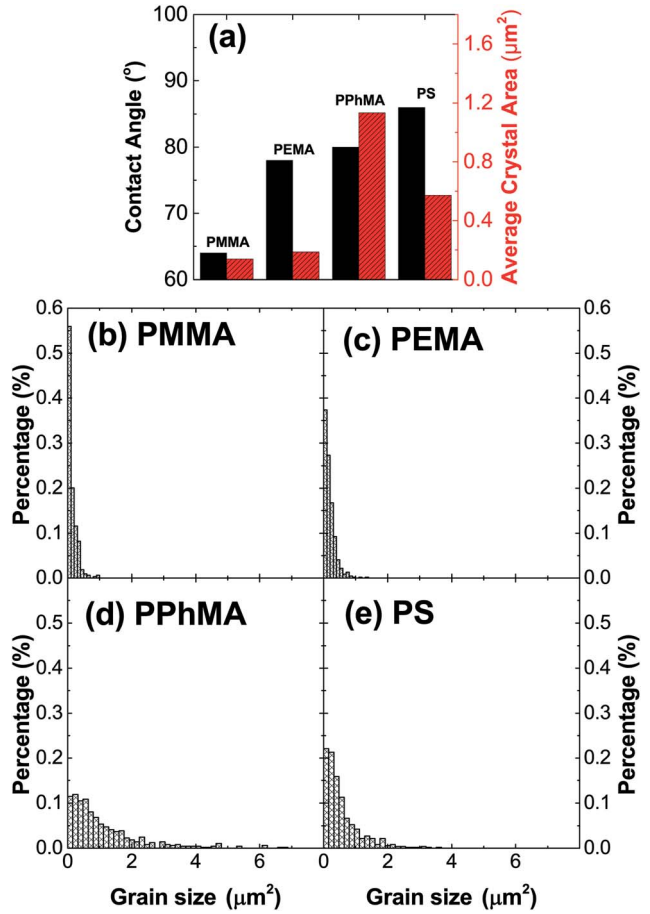

Fig. 4 (a) Relationship between contact angle and average perovskite crystal size on different polymer substrates, with the corresponding distribution histograms of (b) PMMA, (c) PEMA, (d) PPhMA and (e) PS substrates.

The correlation between crystal size and the difference in hydrophobicity can be attributed to the substituent effect on the methacrylate polymer, in an order of methyl < ethyl < phenyl [Fig. 4(a)]. For PiPMA and PiBMA, which have isopropyl and isobutyl substituents respectively, PiPMA gives a poorly-wetting surface where perovskite crystals can hardly form on it, resulting in a poorly developed and non-uniform film [Fig. 3(c)], and PiBMA simply gives a non-wetting surface for the PbI_2 solution [Fig. 3(d)]. On the PiPMA and PiBMA surfaces, the alkyl groups are so bulky that they may hinder the interactions between the O atoms on the MA polymer and the Pb^{2+} ions during the spin-coating process of PbI_2. The longer the alkyl substituent, the greater the steric hindrance for the O atom nucleation sites. Moreover, the electropositive hydrogen atoms in the alkyl groups could appear repulsive to the Pb^{2+} ions. Thus, the electronic interactions between the O atoms and the Pb^{2+} ions would be weakened [Fig. 5]. In other words, the bulky alkyl groups act as a barrier to the adhesion of PbI_2 on the surfaces for crystal nucleation at the early stage of PbI_2 deposition, leading to poor crystal growth on such surfaces. When the substituents are small (*e.g.* methyl and ethyl), as shown in Fig. 5, the inductive effect from these electron donating groups can

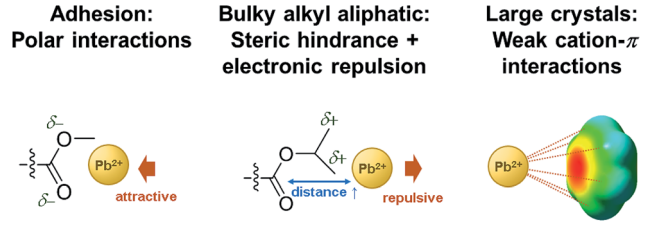

Fig. 5 Different interactions between the moieties in the polymers and the Pb^{2+} ion during the spin-coating process of PbI_2 solution onto them.

enhance the interaction between the O atoms and the Pb^{2+} ions, giving rise to larger crystal sizes. Here, it can be hypothesized that the side groups in the MA moieties can regulate the size and quality of the crystals during the crystal growth process with the SEM and crystal size statistical data [Fig. 3(a), (b) and 4(a)], and that the SEM results of the poorly developed films on PiPMA and the non-wetting surface on PiBMA support the role of the O atoms in the Pb^{2+} ion adhesion on the polymer surfaces by demonstrating the masking effect of the O atoms due to the bulky aliphatic isopropyl and isobutyl groups. It is also important to note that the correlation between the crystal size and surface hydrophobicity should only be valid in the same polymer series.

It is worth noting that, despite the similar hydrophobicity of PiPMA and PPhMA as observed *via* the contact angle measurements, PPhMA gave a well-wetted perovskite film but PiPMA gave a poorly-wetting surface for perovskite growth. Therefore, compared to aliphatic substituents (*e.g.* methyl and ethyl), aromatic substituents (*e.g.* phenyl) provided better benefits of obtaining large and high quality perovskite crystals as shown in the case of PPhMA [Fig. 4(e)]. The beneficial effect of PPhMA on perovskite growth may possibly be due to the additional weak cation–π interactions between the Pb^{2+} ions and the phenyl groups,[24,25] as shown in Fig. 5. Such interaction may assist the perovskite growth during the annealing process, and thus provide extra support to the coordinational crystal growth besides the polar interaction between the O atom nucleation sites and the Pb^{2+} ions. Therefore, the presence of both the O atoms and the phenyl groups functioned synergistically to the crystal growth, resulting in the highest crystal quality and the greatest crystal size. On the other hand, the study of perovskite growth on the hydrophobic PS surface demonstrated the effect of the sole cation–π interactions between the phenyl groups and Pb^{2+} ions without any O atoms as nucleation sites. The perovskite crystals on PS could still be grown owing to the cation–π interactions which helped nucleation. However, the cation–π interaction is much weaker than the interaction between polar electronegative atoms and the Pb^{2+} ions once the perovskite crystal growth was completed. Thus, without the electronegative oxygen atoms in PS, crystal adhesion is significantly weakened and numerous pinholes evenly distributed on the PS surface were found. As for PiPMA and PiBMA, with both the absence of the phenyl groups and the weakened polar interaction from the O atoms due to the bulky and electropositive aliphatic alkyl side

groups, Pb^{2+} adhesion on these surfaces on which perovskite crystals can hardly form is found to be difficult.

In summary, our study found out the following in relation to obtaining large and quality $CH_3NH_3PbI_3$ perovskite polycrystalline films on MA polymers: (1) electronegative O atoms are beneficial to perovskite nucleation events and adhesion of perovskite on the surface; (2) appropriate choices of aliphatic alkyl substituents in the MA group balancing the counteracting inductive effect and steric effect together with repulsively electronic interactions give well-adhered and regulated large perovskite crystal surfaces; and (3) aromatic (phenyl) substituents offer cation–π interactions and help develop large perovskite crystals.

3.2 Electronic properties of the perovskite films

Photothermal deflection spectroscopy results. To assess the electronic properties of the perovskite films on the different polymer insulators, we measured the subgap optical absorptions of these films with photothermal deflection spectroscopy (PDS).[26] PDS is based on the mirage effect. The sample film under investigation is irradiated with a modulated monochromatic light source. Optical absorption by the sample creates a periodic temperature rise in the surrounding medium, and in turn induces a change in the refractive index. A laser beam directed just above the sample will be deflected as a result of the changes in the refractive index. For a small temperature rise, the amount of deflection can be shown to scale with the optical absorption of the film.[27] With the PDS method, the optical absorption of a semiconductor below the bandgap can be obtained by scanning the photon energy of the incident light source. Details of our experimental setup have been reported elsewhere.[28]

Fig. 6 shows the subgap optical absorption of the perovskite films on the different polymers. For each absorption spectrum, a sharp drop in absorption occurs at above 1.6 eV, which matches very well with the known energy gap of $CH_3NH_3PbI_3$.[29] The "steepness" of the absorption just below the bandgap energy can be evaluated by the Urbach model:

$$\alpha = \alpha_0 \exp\left[\frac{h\nu - E_g}{E_u}\right] \quad (1)$$

where α_0 is the absorption coefficient at the bandgap energy E_g, $h\nu$ is the photon energy, and E_u is the Urbach energy. The Urbach energy is a measure of the width of the tail of the localized states. A smaller E_u implies a better semiconductor and reduced localized states. The inset table in Fig. 6 compares the Urbach energies of the perovskite films. It can be seen that the Urbach energies are 24.9, 23.0 and 22.7 meV for perovskite films on PMMA, PEMA and PPhMA, respectively. The magnitude of E_u suggests that the perovskite film grown on PPhMA has the least localized states and the smallest amount of defects. The PDS results are, therefore, generally consistent with the SEM observations which show that the perovskite on PPhMA has the largest crystals. The defects observed in PDS can be associated with reduced grain boundaries of the perovskite on the PPhMA surface.

TFT fabrication and characterization. Encouraged by the film growth from Section 3.1, we used these films for TFT testing. The perovskite TFTs were fabricated using the bottom-gate top-contact (BGTC) scheme as indicated in Fig. 7. Compact perovskite films were fabricated on PMMA, PEMA and PPhMA as outlined in Section 3.1. Onto these films, Au source (*S*)/drain (*D*) electrodes were formed by thermal evaporation. The channel length and width were 50 μm and 6 mm, respectively. The TFTs were tested for both p- and n-type characteristics between 120–290 K. Only n-type behavior can be observed. Fig. 8(a)–(c) show a representative set of perovskite TFT output characteristics on the three different polymer gate dielectric materials at 202 K. Well-behaved output characteristics can be observed for all the devices with clear linear and saturation regions. The saturation mobilities of the perovskite TFTs were evaluated from the transfer characteristics by

$$I_{DS} = \frac{W}{2L} C_i \mu_{sat} (V_G - V_T)^2 \quad (2)$$

where I_{DS} is the source drain current, W and L are the TFT channel width and length, C_i is the capacitance per unit area of the dielectric material, μ_{sat} is the carrier mobility, V_G is the gate voltage and V_T is the threshold voltage. Fig. 8(d) compares their

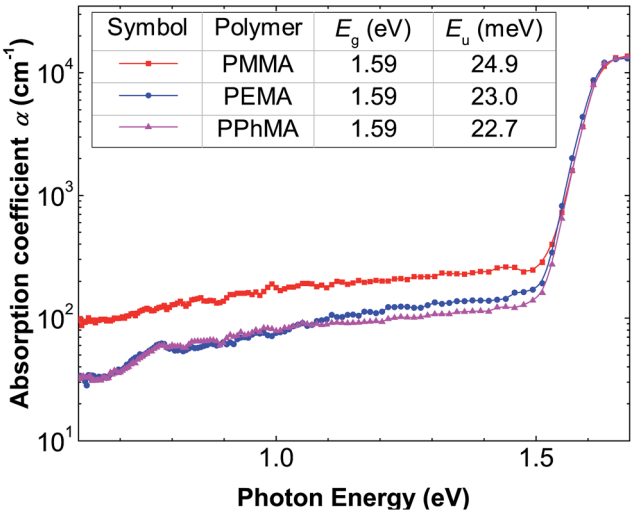

Fig. 6 Photothermal deflection spectra of the perovskite on the different polymer gate dielectric surfaces. The corresponding values of bandgap E_g and Urbach energy E_u are shown in the inset table.

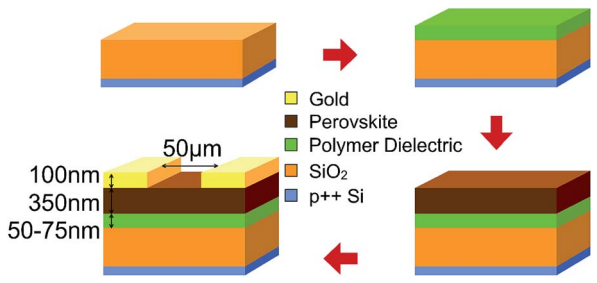

Fig. 7 Schematic diagram showing the fabrication procedure of the bottom-gate-top-contact (BGTC) perovskite TFT devices.

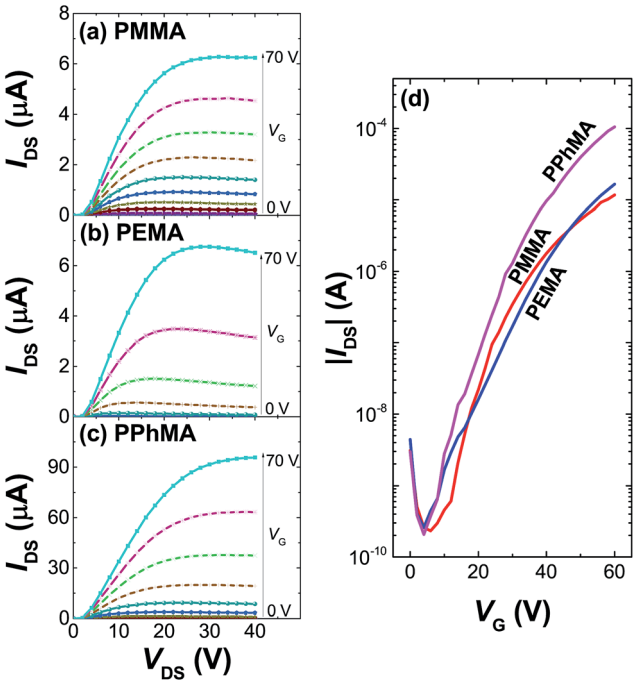

Fig. 8 Output characteristics of the perovskite TFT at 202 K on the (a) PMMA, (b) PEMA and (c) PPhMA polymer substrates. (d) Transfer characteristics at V_{DS} = 40 V of the perovskite TFT at 202 K on the three polymer gate dielectric surfaces.

transfer characteristics. The largest TFT mobility can be observed for the perovskite TFT grown on PPhMA, with significantly steeper transfer characteristics and a value of μ_{sat} = 0.40 $cm^2 V^{-1} s^{-1}$. On the other hand, the mobility is the smallest for the perovskite grown on PEMA with 0.030 $cm^2 V^{-1} s^{-1}$.

Table 1 summarizes the TFT data at 202 K. The electron mobility of the perovskite thin film improves from PEMA < PMMA < PPhMA. Again, the best device corresponds to the perovskite grown on PPhMA. The TFT mobilities for the perovskite on PMMA and PEMA are similar, of the same order of 0.03–0.05 $cm^2 V^{-1} s^{-1}$, possibly due to their similar crystal sizes, despite the slightly larger mobility of PMMA than its PEMA counterpart. For the PPhMA device, the substantially larger crystallites [Fig. 4(a)] implies fewer grain boundaries which enhance charge carrier transport.

The TFT device using PPhMA as the best gate dielectric material was also given an operational stability test. The device was kept at 202 K under high vacuum (10^{-5} Torr) for an extended period of time and the variation of the electron

Table 1 TFT performance including capacitance per unit area C_i, saturation electron mobility μ_{sat}, threshold voltage V_T and on-to-off current ratio $I_{on/off}$ of the $CH_3NH_3PbI_3$ perovskite using the different polymer dielectric materials at 202 K

Dielectric	C_i (nF cm^{-2})	μ_{sat} ($cm^2 V^{-1} s^{-1}$)	V_T (V)	$I_{on/off}$
PMMA	9.06	0.056	31.6	5.0×10^4
PEMA	8.89	0.030	45.7	1.3×10^5
PPhMA	9.19	0.40	34.3	5.1×10^5

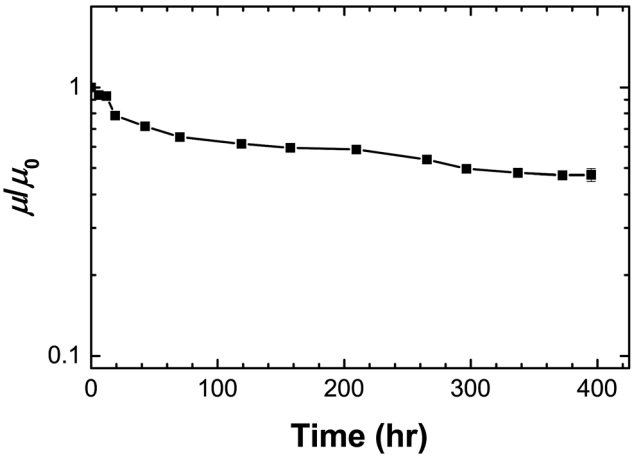

Fig. 9 Operational stability of the TFT device at 202 K using PPhMA as the gate dielectric material. μ/μ_0 is the normalized mobility.

mobility was recorded as shown in Fig. 9. After an initial slight drop, the electron mobility retained little decrease even after 400 hours despite the electrical stress given during the repeated measurements. The half-life of the device is estimated as 300 hours. The operational stability of the device without engineering-level optimization was preliminarily found encouraging, and further work can be done on enhancing its tolerance under electrical stress.

Finally, we want to briefly comment on how temperature influences charge transport in perovskite transistors. In the low

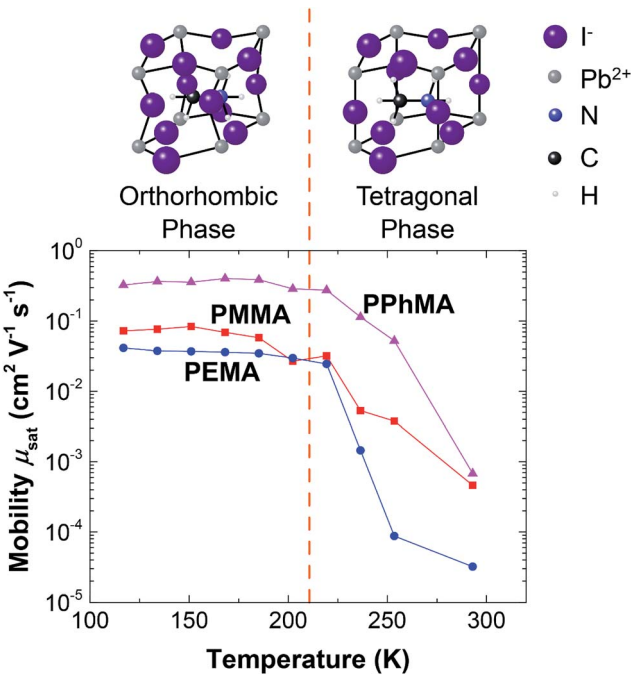

Fig. 10 Electron mobility against temperature of the perovskite TFT using the different gate dielectric materials. The models on top indicate the different phases of $CH_3NH_3PbI_3$ at different temperature regions.

temperature regime, as the temperature is reduced from 200 K towards 100 K, a gentle increase in the mobility was observed. The increase in mobility in this temperature range can be attributed to the reduction of lattice scattering or phonon vibrations of the crystals. However, as T increases to above 250 K, a significant reduction in mobility occurs for all samples. At room temperature, mobilities are reduced by at least 2 orders. The sharp reduction in mobility starting at 250 K can be attributed to the phase transition of the perovskite crystals from the orthorhombic phase to the tetragonal phase as depicted in Fig. 10.[19] Furthermore, it was suggested that the electron mobility and unit cell structure are correlated.[14,30,31] From Fig. 10, it can be seen that the cage size of the tetragonal phase is relatively large, and so the structure facilitates the motions of the iodide or methylammonium ions. These ions give rise to electronic disorder that can trap electrons or scatter electron motions. Thus, electron transport is severely affected by these relatively mobile ions in the tetragonal phase.

4 Conclusions

The growth and electronic qualities of methylammonium lead iodide polycrystalline film on several methyl methacrylate-based polymer insulators were investigated. We found that the film growth *via* solution processing is a competition between film adhesion and crystal size. The less hydrophobic methacrylate-based polymer favors film formation but results in films with small crystallites with an island area of about 0.2 μm^2. More hydrophobic polymers potentially result in much larger but non-adhering crystals. Among the methacrylate-based polymers tested, PPhMA offers the best compromise. It possesses the necessary O atoms in the methacrylate groups for inducing the initial nucleation of the precursor PbI_2, and at the same time, the presence of the phenyl ring provides cation–π interactions between the polymer surface and Pb^{2+} ions with good hydrophobicity to favor large crystal growth. Perovskite films grown on PPhMA surfaces result in the largest and tightly packed crystallites, with an average size of 1.1 μm^2. Electronic evaluation of these films indicates a sharp bandgap at 1.6 eV and the smallest Urbach energy of 22.7 meV. Using perovskites on PPhMA as the active layer for TFTs, an impressive TFT mobility of 0.40 $cm^2 V^{-1} s^{-1}$ can be achieved. The findings here may allow future researchers to develop new polymer additives that can assist or promote perovskite crystal growth in specific morphologies for varied device applications.

Conflicts of interest

There are no conflicts to declare.

Acknowledgements

Support of this research by the research committee of HKBU and the Research Grant Council of Hong Kong under Grant #'s FRG2/14-15/092, HKBU211913 and HKBU12201914 is gratefully acknowledged.

References

1 D. Bi, C. Yi, J. Luo, J.-D. Décoppet, F. Zhang, S. M. Zakeeruddin, X. Li, A. Hagfeldt and M. Grätzel, *Nat. Energy*, 2016, **1**, 16142.
2 Y. Zhao and K. Zhu, *Chem. Soc. Rev.*, 2016, **45**, 655–689.
3 S. Yang, W. Fu, Z. Zhang, H. Chen and C.-Z. Li, *J. Mater. Chem. A*, 2017, **5**, 11462–11482.
4 J.-P. Correa-Baena, A. Abate, M. Saliba, W. Tress, T. J. Jacobsson, M. Grätzel and A. Hagfeldt, *Energy Environ. Sci.*, 2017, **10**, 710–727.
5 A. Dualeh, N. Tétreault, T. Moehl, P. Gao, M. K. Nazeeruddin and M. Grätzel, *Adv. Funct. Mater.*, 2014, **24**, 3250–3258.
6 Y.-X. Chen, Q.-Q. Ge, Y. Shi, J. Liu, D.-J. Xue, J.-Y. Ma, J. Ding, H.-J. Yan, J.-S. Hu and L.-J. Wan, *J. Am. Chem. Soc.*, 2016, **138**, 16196–16199.
7 Y. Cheng, H.-W. Li, J. Qing, Q.-D. Yang, Z. Guan, C. Liu, S. H. Cheung, S. K. So, C.-S. Lee and S.-W. Tsang, *J. Mater. Chem. A*, 2016, **4**, 12748–12755.
8 Q. Lin, A. Armin, R. C. R. Nagiri, P. L. Burn and P. Meredith, *Nat. Photonics*, 2015, **9**, 106–112.
9 Q. Dong, Y. Fang, Y. Shao, P. Mulligan, J. Qiu, L. Cao and J. Huang, *Science*, 2015, **347**, 967–970.
10 Y. Liu, Z. Yang, D. Cui, X. Ren, J. Sun, X. Liu, J. Zhang, Q. Wei, H. Fan, F. Yu, *et al.*, *Adv. Mater.*, 2015, **27**, 5176–5183.
11 H. Sirringhaus, *Adv. Mater.*, 2014, **26**, 1319–1335.
12 Z. Bao and J. Locklin, *Organic field-effect transistors*, CRC press, 2007.
13 C. Reese, M. Roberts, M. M. Ling and Z. Bao, *Mater. Today*, 2004, **7**, 20–27.
14 T. Zhao, W. Shi, J. Xi, D. Wang and Z. Shuai, *Sci. Rep.*, 2016, **6**, 19968.
15 A. Chilvery, S. Das, P. Guggilla, C. Brantley and A. Sunda-Meya, *Sci. Technol. Adv. Mater.*, 2016, **17**, 650–658.
16 D. Li, G. Wang, H.-c. Cheng, C.-y. Chen, H. Wu, Y. Liu, Y. Huang and X. Duan, *Nat. Commun.*, 2016, **7**, 11330.
17 G. Wang, D. Li, H.-C. Cheng, Y. Li, C.-Y. Chen, A. Yin, Z. Zhao, Z. Lin, H. Wu, Q. He, *et al.*, *Sci. Adv.*, 2015, **1**, e1500613.
18 F. Li, C. Ma, H. Wang, W. Hu, W. Yu, A. D. Sheikh and T. Wu, *Nat. Commun.*, 2015, **6**, 8238.
19 X. Y. Chin, D. Cortecchia, J. Yin, A. Bruno and C. Soci, *Nat. Commun.*, 2015, **6**, 7383.
20 Y. Mei, C. Zhang, Z. V. Vardeny and O. Jurchescu, *MRS Commun.*, 2015, **5**, 297–301.
21 C. Bi, Q. Wang, Y. Shao, Y. Yuan, Z. Xiao and J. Huang, *Nat. Commun.*, 2015, **6**, 7747.
22 D. Zhao, M. Sexton, H.-Y. Park, G. Baure, J. C. Nino and F. So, *Adv. Energy Mater.*, 2015, **5**, 1401855.
23 T. Salim, S. Sun, Y. Abe, A. Krishna, A. C. Grimsdale and Y. M. Lam, *J. Mater. Chem. A*, 2015, **3**, 8943–8969.
24 J. C. Ma, D. A. Dougherty, *et al.*, *Chem. Rev.*, 1997, **97**, 1303–1324.
25 N. Zacharias and D. A. Dougherty, *Trends Pharmacol. Sci.*, 2002, **23**, 281–287.

26 W. B. Jackson, N. M. Amer, A. Boccara and D. Fournier, *Appl. Opt.*, 1981, **20**, 1333–1344.
27 A. Boccara, W. Jackson, N. M. Amer and D. Fournier, *Opt. Lett.*, 1980, **5**, 377–379.
28 C. H. Y. Ho, S. H. Cheung, H.-W. Li, K. L. Chiu, Y. Cheng, H. Yin, M. H. Chan, F. So, S.-W. Tsang and S. K. So, *Adv. Energy Mater.*, 2017, **7**, 1602360.
29 G. E. Eperon, S. D. Stranks, C. Menelaou, M. B. Johnston, L. M. Herz and H. J. Snaith, *Energy Environ. Sci.*, 2014, **7**, 982–988.
30 S. P. Senanayak, B. Yang, T. H. Thomas, N. Giesbrecht, W. Huang, E. Gann, B. Nair, K. Goedel, S. Guha, X. Moya, *et al.*, *Sci. Adv.*, 2017, **3**, e1601935.
31 P. S. Whitfield, N. Herron, W. E. Guise, K. Page, Y. Q. Cheng, I. Milas and M. K. Crawford, *Sci. Rep.*, 2016, **6**, 35685.